Clinical advances in cardiovascular magnetic resonace imaging and angiography

Bosch, H.C.M. van den

Chapter 2

CMR: Imaging Planes and Anatomy

Harrie CM van den Bosch
Jos JM Westenberg
Albert de Roos

based on
Chapter 7 CMR: Imaging Planes and Anatomy
in MRI and CT of the Cardiovascular System, 3rd Edition, 2013
Charles B Higgins and Albert de Roos
Lippincott Williams & Wilkens

Cardiac magnetic resonance (CMR) imaging has the ability to provide arbitrary views of the cardiac structures which can be chosen freely since this modality is not hampered by the availability of acoustic windows, as in echocardiography. Even though echocardiography, x-ray LV angiography, and cardiac computed tomography (CT) are nowadays commonly used techniques for evaluating cardiac disease in clinical practice, CMR has evolved to become the preferential technique for anatomic and functional cardiac imaging.

Two-dimensional (2D), single-plane, multiple-2D, or three-dimensional (3D) imaging is possible with CMR. Furthermore, temporal information of the dynamics of the heart can be provided as imaging is synchronized to the cardiac frequency, using either prospective triggering or retrospective gating.[1] With prospective triggering, the operator will set the expected heart rate before the acquisition and triggering will be performed according to this chosen heart rate. With retrospective gating, imaging is performed continuously and additionally the ECG signal will be stored. In retrospect, k-space filling is synchronized to the stored ECG. This synchronization enables time-resolved imaging and multiple phases of the cardiac cycle can be obtained. The acquired views in multiple phase of the heart can be presented in cine mode, providing functional information on the temporal behavior of the cardiac structures.

Imaging planes in CMR are usually obtained in the orientation to the axes of the heart, or oriented to the major axes of the body. Therefore, the standard CMR planes of the heart are comparable to the standard cardiac views known and established in other noninvasive imaging modalities such as echocardiography, cardiac CT, x-ray LV angiography, and nuclear techniques (e.g., single-photon emission computed tomography [SPECT] and positron emission tomography [PET]). Compared to cardiac CT, x-ray angiography, and nuclear techniques, CMR allows noninvasive, high-resolution imaging without using ionizing radiation. Furthermore, the morphology of the right ventricle (RV) is excellent delineated by CMR, whereas in echocardiography the assessment of RV geometry and function is challenging because of the particular crescentic shape of the RV wrapping around the left ventricle (LV).[2]

The choice for a specific scan protocol is mainly determined by the diagnostic question which has to be answered. In CMR imaging, both static and dynamic images of the heart can be acquired. Therefore, it is important to be adequately informed by the referring clinician prior to the CMR examination. Standardized nomenclature for cross-sectional anatomy has been described,[3] facilitating comparison between different techniques and proper communication in clinical practice. The 17-segment model of the LV, proposed by the American Heart Association (AHA), is nowadays widely used and accepted in clinical CMR imaging, as in other cross-sectional imaging modalities (e.g., cardiac CT and nuclear techniques). The recommended model comprehends six basal segments, six mid-ventricular segments, four apical (distal) segments, and one true apex (Figure 2.1). These 17 segments are routinely evaluated when regional LV performance is questioned.

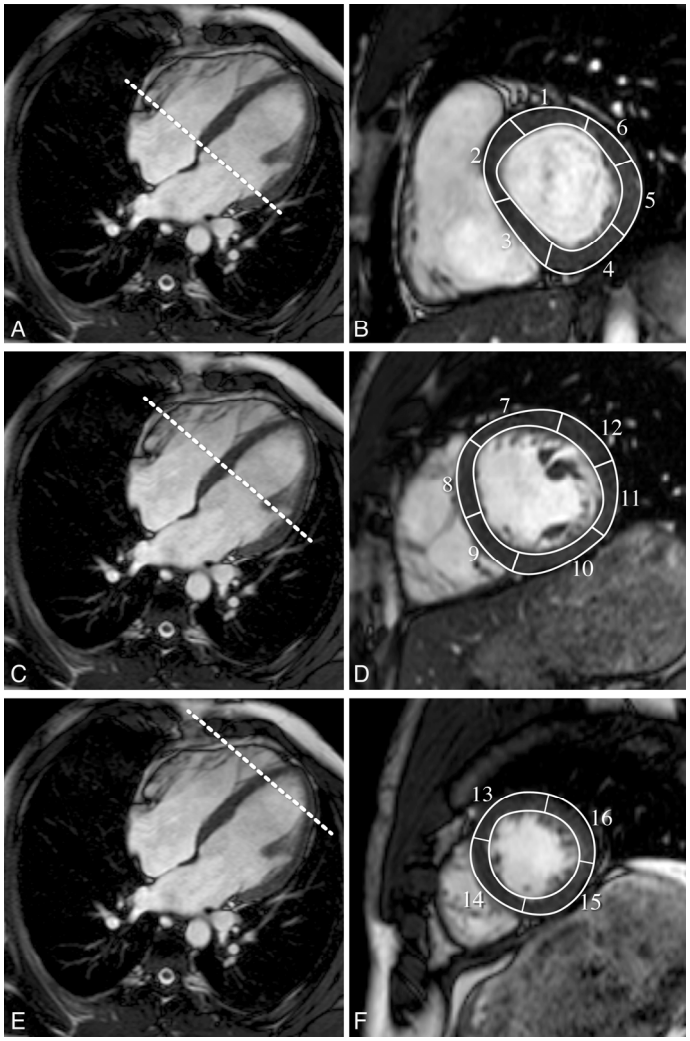

Figure 2.1 The standardized 17 segments of LV as proposed by the American Heart Association. At basal **(B)** and mid-ventricular **(D)** level, the myocardium is divided into six segments each, and at apical **(F)** level, the myocardium is divided into four segments. Nomenclature: Segment 1, basal anterior; 2, basal anteroseptal; 3, basal inferoseptal; 4, basal inferior; 5, basal inferolateral; 6, basal anterolateral; 7, midanterior; 8, mid-anteroseptal; 9, mid-inferoseptal; 10, mid-inferior; 11, mid-inferolateral; 12, mid-anterolateral; 13, apical anterior; 14, apical septal; 15, apical inferior; 16, apical lateral. Segment 17 (not presented) is the true apex, which can be evaluated on a long-axis view. Dashed lines on the four-chamber view **(A**,**C**, and **E)** indicate the planning of the acquisition level.

Another important issue in clinical CMR imaging is the ability of the patient to cooperate during the examination and to perform breath-holding. If a patient is capable to perform breath-holding, successive scan planes are obtained with accelerated imaging, with the patient usually performing breath-holding in expiration. Preferably, image planes in CMR imaging are acquired in mid- or end-expiration, as the anatomic level may be obtained more reproducible compared to planes which are scanned in inspiration.[4]

For planning purposes, new generation clinical MR scanners provide the possibility to plan the various scan planes interactively with real-time imaging. During free-breathing CMR, planning can be performed accurately. After all scan planes are defined and obtained interactively, the acquisition of the cine long-axis (LA) and short-axis (SA) views may be performed during breath-holding. This interactive approach for planning is fast, reliable, and patient friendly, and essential in patients who are not capable to hold their breath consecutively, for example, patients with respiratory disease or with heart failure. Fully automated CMR planning methods have also been described and can provide accurate and reproducible measurements of LV dimensions.[5]

With CMR, the choice of scanning technique is aimed at the choice between bright-blood and black-blood imaging, which essentially determines the contrast between myocardium and the intra-cardiac blood pool. For the assessment of left and right ventricular function, fast gradient-echo sequences are usually performed in combination with steadystate free precession (SSFP) technique (balanced-TFE, True-FISP, Fiesta) for optimal contrast. On these images, the blood pool is presented with bright signal whereas the myocardium is represented dark with low signal. This results in an excellent definition of the LV endocardial and epicardial borders, which is required for accurate image segmentation during cardiac volume and function quantification Typically, SSFP images should be acquired with slice thickness of 6 to 8 mm and temporal resolution better than 45 milliseconds to obtain optimal accuracy in ventricular function assessment.[6,7]

In addition, cardiac morphology can be evaluated by double-inversion, black-blood, spin-echo sequences with fat suppression, providing static images of the heart with high spatial resolution (optimally, in-plane acquired resolution of better than 2x2 mm and slice thickness of 5 to 8 mm) in the orientation of the heart or the patient's body axes. These images are, for example, obtained in the work-up of congenital heart disease or cardiac tumors (Figure 2.2).

In the remainder of this chapter, the planning of the specific imaging planes will be discussed, as well as the normal cardiac structures that are visualized. Furthermore, the aspects of cardiac imaging on (ultra-) high-field MRI will be addressed.

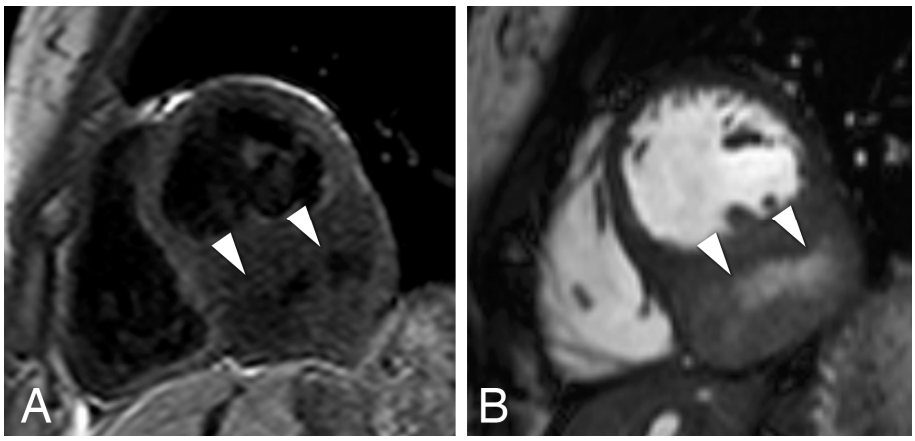

Figure 2.2 Black-blood **(A)** and bright-blood **(B)** short-axis acquisition illustrating a cardiac sarcoma (*arrow heads*) in the inferior wall, acquired in a 19-year-old female.

Cardiac Axis Imaging Planes

To acquire imaging planes in the direction of the cardiac axes, multi-stack, single-shot SSFP scout views are used for planning. If available, free-breathing real-time scanning can be used instead that is advantageous for patient's comfort. Perpendicular to an anatomical transverse image, displaying the heart's four chambers, an acquisition plane is chosen through the middle of the atrioventricular junction at the level of the mitral valve and running through the apex (Figure 2.3). This plane is the so-called vertical long-axis (VLA) plane. On this VLA view, a plane is defined intersecting the apex and the middle of the mitral valve, resulting in the horizontal long-axis (HLA) view. The HLA view is almost comparable to the four-chamber view; however, in this HLA view often a part of the LV outflow tract (LVOT) is visualized. On the acquired HLA plane, the SA views covering the entire LV are planned parallel to the ring of the mitral valve and perpendicular to the line intersecting the apex.
For reasons of reproducibility and comparison, the true two- and four-chamber view can still be obtained. The twochamber view is planned perpendicular to the anterior and inferior wall of the LV through the center of the LV cavity on a mid-ventricular SA image intersecting the apex. On the two-chamber view, the apex, anterior and inferior wall of the LV, the mitral valve, and left atrium can be analyzed (Figure 2.4A). The four-chamber view is planned also on a mid-ventricular SA image by a plane through the center of the LV cavity and the acute margin of the RV, also intersecting the apex. The four-chamber view depicts the inferior interventricular septum, the anterior

lateral wall of the LV, the free wall of the RV, left and right atrium as the interatrial septum, and both the mitral and tricuspid valves (Figure 2.4B).

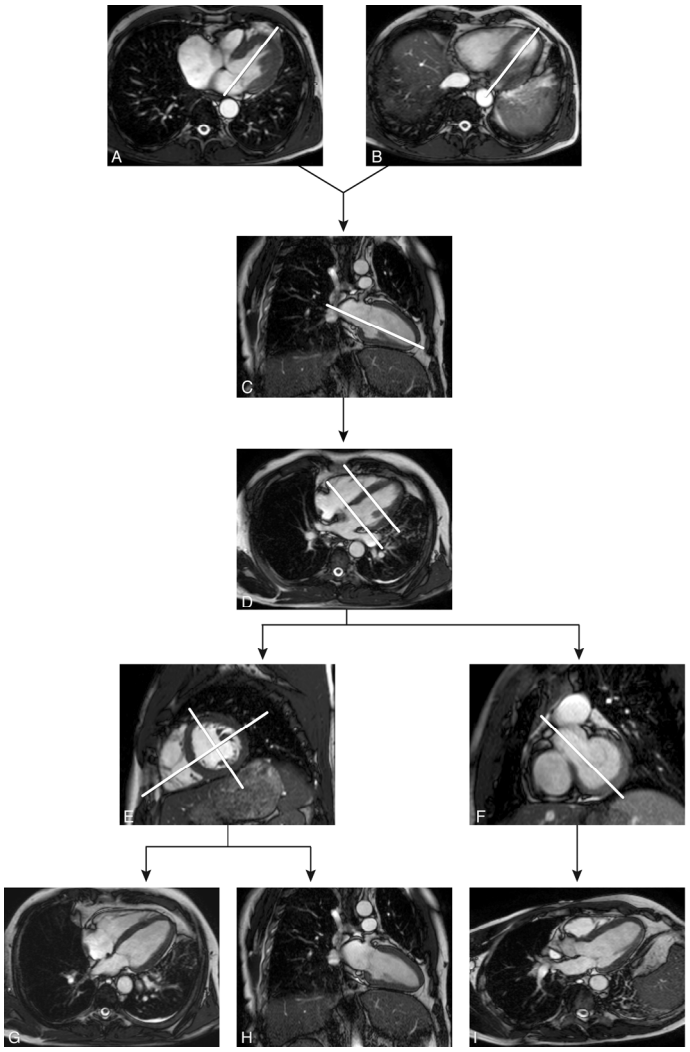

Figure 2.3 Planning acquisition of standard cardiac views. On two transverse slices **(A)** and **(B),** the left ventricular vertical long-axis (VLA) **(C)** is planned by a plane transecting the mitral valve and the apex. The horizontal long-axis (HLA) **(D)** is obtained by acquiring a plane transecting the VLA through the mitral valve and apex. A short-axis image can be obtained perpendicular to HLA, at mid-ventricular **(E)** and basal level **(F).** The four-chamber **(G)** of the LV is obtained as indicated from a plane transecting both LV and RV. The two-chamber **(H)** of the LV is acquired perpendicular to the fourchamber. The three-chamber LV **(I)** is obtained from a plane transecting the LV through the LVOT.

Routinely, the three-chamber or the so-called LVOT view is planned perpendicular to a basal SA plane. This view also intersects the apex. The LVOT view (Figure 2.4C) depicts the apex, the anterior interventricular wall, the LVOT, the inferior lateral wall, as the aortic and mitral valve, respectively. The standard SSFP cine CMR protocol for assessing LV function should include the two-, four-, and three-chamber views in combination with SA images covering the entire LV, resulting in scans covering all described 17 LV segments in two directions.

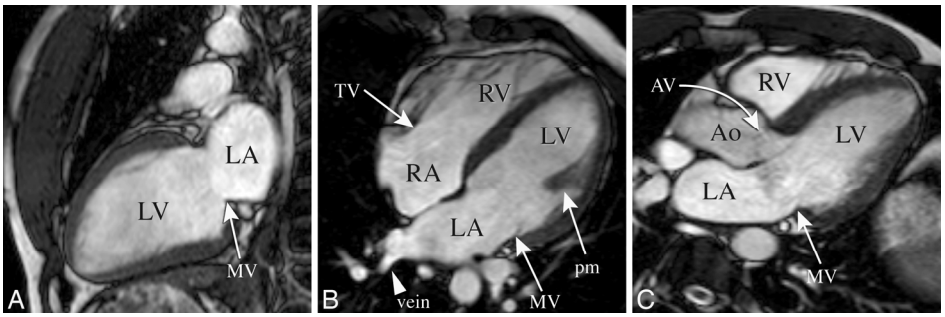

Figure 2.4 Normal cardiac anatomy on two-**(A)**, four**(B)**-, and three-chamber **(C)** views. LA, left atrium; LV, left ventricle; MV, mitral valve; TV, tricuspid valve; RV, right ventricle; RA, right atrium; pm, papillary muscle; AV, aortic valve; Ao, aorta.

In addition, the RV outflow tract can be obtained. This view can be planned on a coronal image, depicting the outflow tract of the RV. Alternatively, an optimized view of the RV outflow tract view can be obtained from a plane outlining the tricuspid valve plane and the outflow tract. On this plane, the outflow tract, pulmonary valve, tricuspid valve, and the basal (diaphragmatic) part of the RV wall are all visualized (Figure 2.5).

Body Axes Imaging Planes

For the evaluation of cardiac morphology, the pericardium, the great thoracic vessels, and (para-)cardiac masses imaging planes can be used oriented to the main body axes. Also, the transverse (or axial), coronal (frontal), and sagittal planes are well known to surgeons and other clinicians, as these anatomic orientations are similar to clinical (cardiac) CT. Black- and bright-blood sequence approaches (Fig. 7.6) can be used in optimally adjusted planes to answer specific clinical questions. These imaging sequences provide static images in single phase, not suitable for quantification of LV

or RV dimensions, as end-diastolic diameters or wall thickness. For this analysis, SSFP multiphase images with appropriate temporal resolution are more suitable.

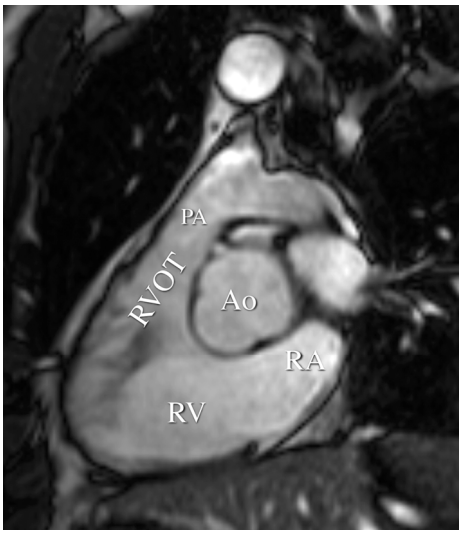

Figure 2.5 Bright-blood acquisition of the right ventricle, illustrating the right ventricular outflow tract (RVOT). PA, pulmonary artery; RVOT, right ventricular outflow tract; Ao, aorta; RA, right atrium; RV, right ventricle.

Transversely oriented planes (Figure 2.7) are especially useful for the evaluation of thoracic vascular structures as the ascending and descending thoracic aorta, the superior and inferior vena cava, the pulmonary trunk, and right and left pulmonary artery. The right and left pulmonary veins (PVs) entering the left atrium are also well depicted. Images in transverse orientation through the heart allow studying morphology of the ventricles and atria, as their internal relationship. Also the RV free wall, the RV outflow tract (infundibulum), the pericardium, and mediastinum are well depicted. It has been described that RV volume and function quantification by planimetry can be performed more accurately on transversely oriented images instead of SA images.[8]

Coronal or frontal anatomic views can be very instructive to analyze the connection between the heart and the great vessels. In the heart, the LVOT and the left atrium with its branches are clearly imaged. An advantage of the frontal view is the similarity to the chest x-ray, well known to the clinicians. On sagittal images, the RV outflow tract in relation to the pulmonary valve is well outlined and the connection of the right atrium with the superior and inferior vena cava can be studied.

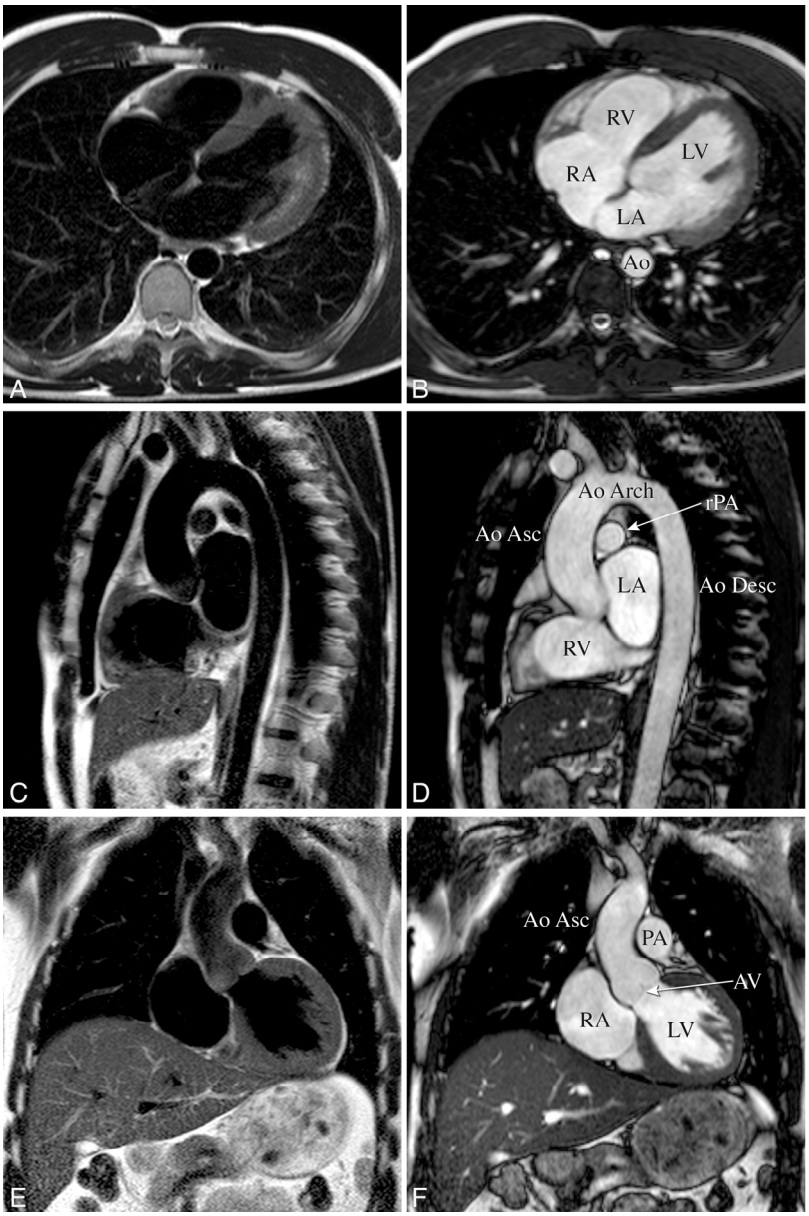

Figure 2.6 Normal cardiac anatomy on black-blood and brightblood acquisitions, in transverse **(A** and **B)**, sagittal **(C** and **D)**, and coronal **(E** and **F)** views. RV, right ventricle; LV, left ventricle; RA, right atrium; LA, left atrium; Ao, aorta; rPA, right pulmonary artery; Ao Asc, ascending aorta; LA, left atrium; RV, right ventricle; Ao Desc, descending aorta; PA, pulmonary artery; AV, aortic valve.

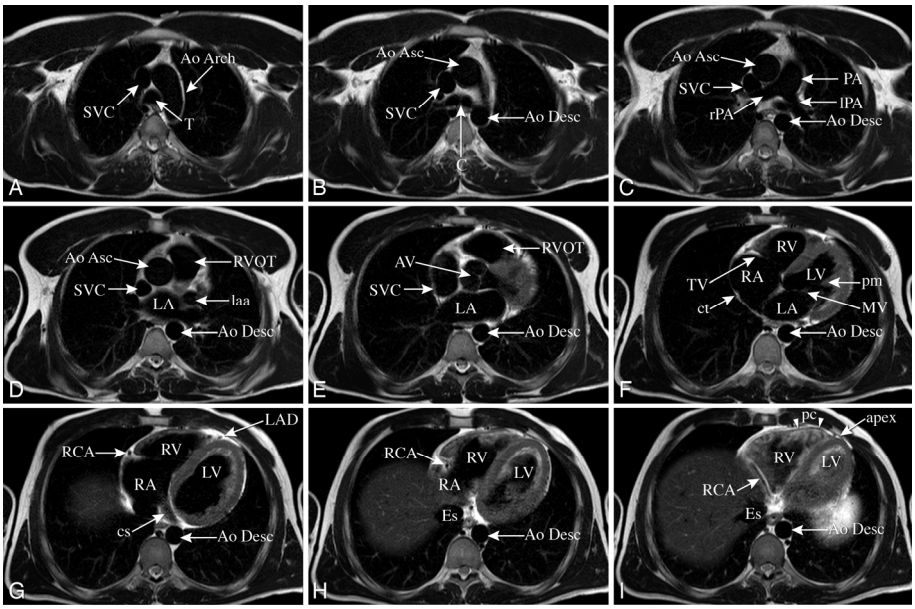

Figure 2.7 Normal cardiac anatomy on transverse black-blood acquisitions. SVC, superior vena cava; T, trachea; Ao Asc, ascending aorta; Ao Desc, descending aorta; C, carina; rPA, right pulmonary artery; PA, pulmonary artery; lPA, left pulmonary artery; LA, left atrium; RVOT, right ventricular outflow tract; LA, left atrium; laa, left atrial appendage; AV, aortic valve; RV, right ventricle; RA, right atrium; TV, tricuspid valve; LV, left ventricle; pm, papillary muscle; MV, mitral valve; LAD, left arterial descending coronary artery; RCA, right coronary artery; cs, coronary sinus; ct, crista terminalis; Es, esophagus; pc, pericard.

Anatomy

CMR images present distinct anatomic features of both atria and ventricles. New generation MRI scanners provide morphologic characteristics in great detail and CMR images are used to evaluate cardiac anatomy in patients with complex cardiac anomalies. For evaluation, either transverse (Figure 2.7) or longitudinal planes, SA (Figure 2.8) or LA cardiac views can be chosen.

The pericardial sac encloses the heart and the roots of the great vessels. The pericardium consists of two layers. The outer fibrous pericardium is attached anteriorly to the sternum, posteriorly to the thoracic spine, and inferiorly to the diaphragm. The inner, serous pericardium can be divided into a parietal and a visceral layer. The parietal layer of the inner pericardium is closely attached to the outer fibrous pericardium. The visceral layer forms the epicardium, covering the epicardial surface of the heart and the epicardial fat and coronary arteries. The pericardial cavity

is outlined by the parietal and visceral layer of the inner pericardium. Normal pericardium presents a low-signal intensity on MRI, and can be well visualized by surrounding epicardial and pericardial fat. Normally, the pericardium measures less than 4 mm on CMR images. Posteriorly to the ascending aorta reaches the superior pericardial recess. Effusion in this recess has to be differentiated from mediastinal pathology, for example, lymphadenopathy.

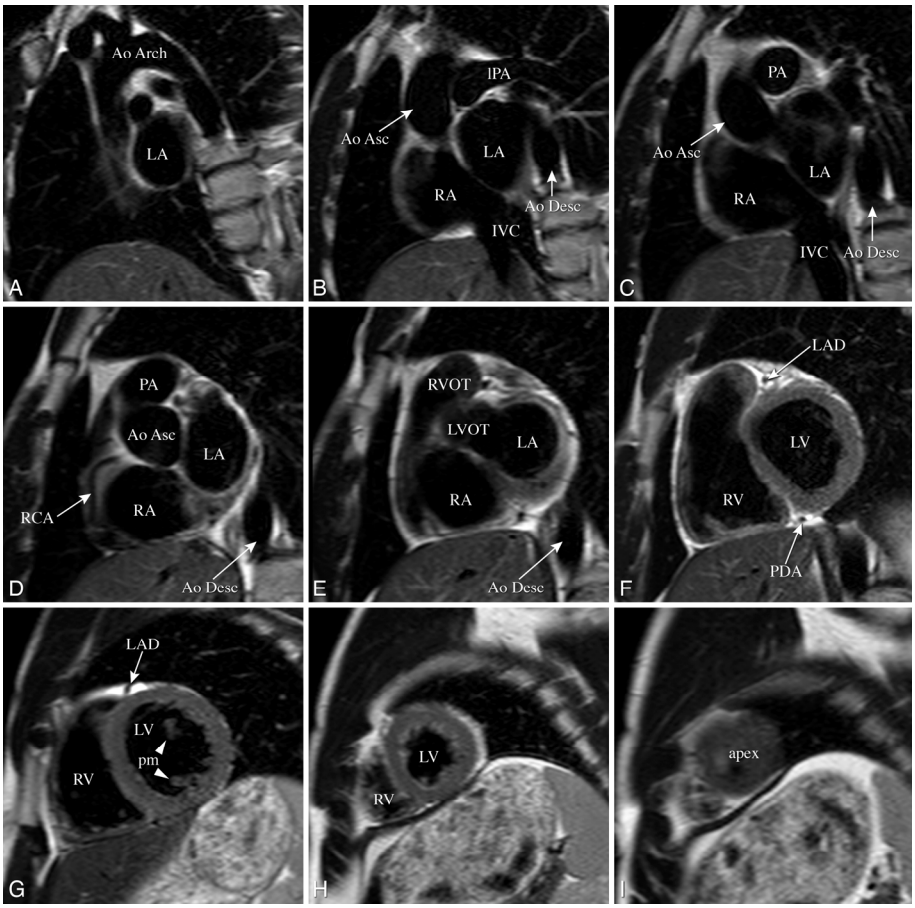

Figure 2.8 Normal cardiac anatomy on shortaxis, black-blood acquisitions. LA, left atrium; lPA, left pulmonary artery; Ao Asc, ascending aorta; RA, right atrium; Ao Desc, descending aorta; IVC, inferior vena cava; PA, pulmonary artery; RCA, right coronary artery; RVOT, right ventricular outflow tract; LVOT, left ventricular outflow tract; LAD, left arterial descending coronary artery; LV, left ventricle; RV, right ventricle; PDA, posterior arterial descending coronary artery; pm, papillary muscle.

In normal cardiac anatomy the right atrium can be recognized by a broad-based triangular appendage. At the base, the tricuspid valve, positioned between the right atrium and the RV, is located closer to the apex when compared to the mitral valve on the left side. The right atrium receives venous blood from the superior and inferior vena cava, and the coronary sinus. The coronary sinus enters the right atrium in the posterior atrioventricular groove. In the right atrium, the Eustachian valve (Ev) (Figure 2.9) can be recognized at the orifice of the inferior vena cava. The crista terminalis separates the anterior and posterior part, two embryologic distinctive parts of the right atrium. The crista terminalis can present diverse, as prominent, broad-based or thin, valve-like (Figure 2.10). Chiari's network is another normal anatomic variant that can be identified. Chiari's network is a congenital remnant of the right valve of the sinus venosus, in literature a prevalence of 1.5% to 2% has been described.[9]

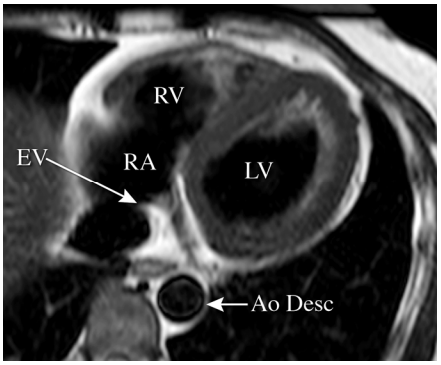

Figure 2.9 Transverse black-blood acquisition illustrating the Eustachian valve. RV, right ventricle; Ev, Eustachian valve; RA, right atrium; LV, left ventricle; Ao Desc, descending aorta.

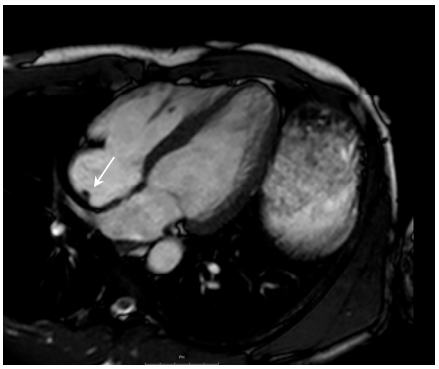

Figure 2.10 Four-chamber bright-blood acquisition illustrating a prominent crista terminalis (arrow head) in the right atrium.

The appendage of the left atrium has a narrow attachment to the atrium and is more tubular shaped. Characteristically, the left atrium receives in total four PVs, two on both sides, although several variations of this occur. Nowadays, imaging the venous anatomy of the heart is becoming more relevant. Moreover, in the preablation work-up the referring clinician needs to be informed about the exact anatomy of the left atrium and spatial orientation of the PV ostia. In patients with atrial fibrillation, MR or CT images of the left atrium and PVs are used to guide the interventional procedure, and provide indispensable information regarding PV anatomy, ostial dimensions, and shape.[10,11] Three-dimensional MR or CT reconstructions of the left atrium can be superimposed on fluoroscopy images during the interventional procedure, thereby facilitating optimal catheter positioning and improving procedural results.[12]
The interatrial septum separates the two atria and can be appreciated as a thin line. As part of the interatrial septum, the fossa ovalis is very thin and can hardly be depicted on CMR images due to the limited spatial acquisition resolution. In some patients, the septum may be infiltrated by lipomatous tissue and thereby thickened (Figure 2.11) or show localized bulging (aneurysm).

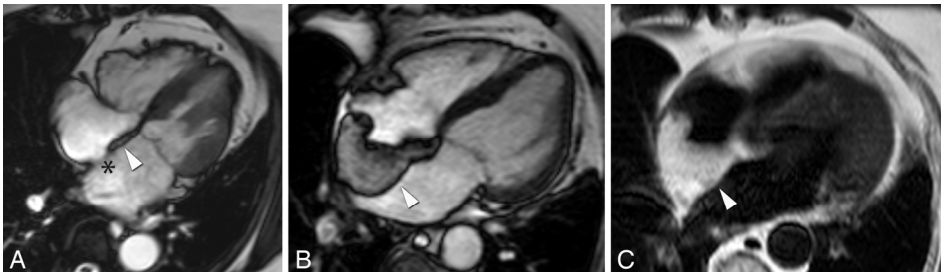

Figure 2.11 Four-chamber, bright-blood **(A** and **B)** and black-blood **(C)** acquisitions, illustrating lipomatous hypertrophy of the intra-atrial septum (arrow heads). The fossa ovalis is indicated by star.

The RV is normally triangular in shape and anteriorly orientated to the right. Morphologically, the RV has typical features that can be depicted on CMR images. The RV shows a muscular moderator band (Figure 2.12), carrying branches of the conducting system. Also, the RV contains a muscular outflow tract (infundibulum or conus arteriosus) and typically, the RV wall is more trabeculated as compared to the LV. In normal anatomy, the LV is positioned posteriorly and LVOT lacks a muscular wall. The interventricular septum consists of a muscular and membranous part. Especially, the membranous part is very thin and sometimes not depicted on CMR images.

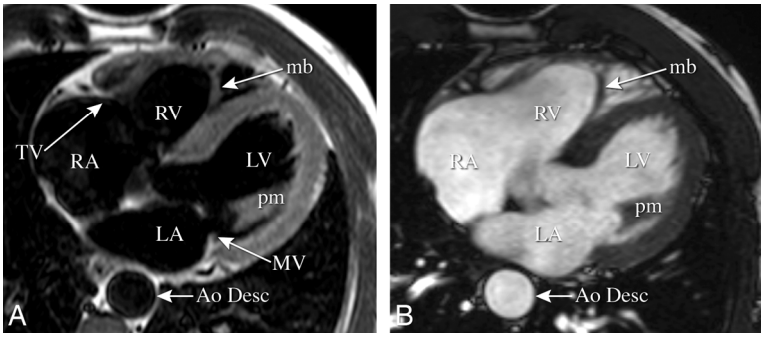

Figure 2.12 Transverse black-blood **(A)** and bright-blood **(B)** acquisitions illustrating the moderator band (mb) in the right ventricle. mb, moderator band; RV, right ventricle; TV, tricuspid valve; RA, right atrium; LV, left ventricle; pm, papillary muscle; LA, left atrium; MV, mitral valve; Ao Desc, descending aorta.

At the outlet of each of the four chambers of the heart, one-way valves are positioned that ensure blood flow in the proper direction. The blood flow through the atria into the ventricles is regulated by the atrioventricular valves: The tricuspid valve on the right side and the mitral valve on the left side, respectively. The pulmonary valve guards the outflow tract of the RV toward the pulmonary trunk, and the aortic valve connects the LVOT to the thoracic aorta. The tricuspid valve comprises three cusps, whereas the mitral valve exists of two cusps. Both the pulmonary and the aortic valve (Figure 2.13) consist of three cusps.

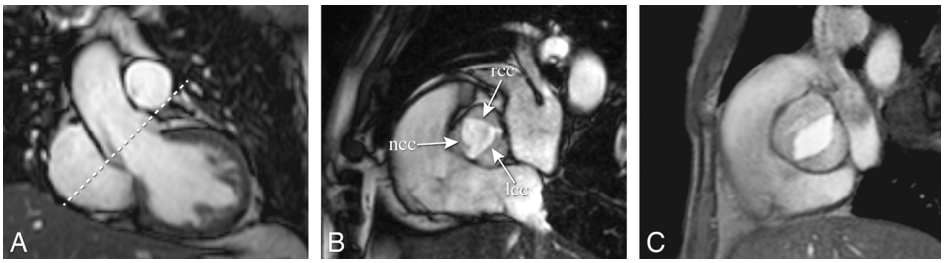

Figure 2.13 A segmented gradient-echo acquisition illustrating the aortic valve area at peak systole. In **(A)**, the planning of the acquisition plane is presented (*dotted line*). In **(B)**, a normal valve with three cusps is presented (lcc, left coronary cusp; rcc, right coronary cusp; ncc, noncoronary cusp), while in **(C)**, a bicuspid aortic valve is presented, with a fused noncoronary and left coronary cusp.

Opening of the atrioventricular valves is predominantly determined by pressure differences between the atria and ventricles. These differences are the result of the isovolumic relaxation of the ventricles. Furthermore, the motion of the valves is regulated by papillary muscles, which originate from the inferior myocardial wall and are connected to the valve leaflets by chordae tendineae. During contraction of the ventricle the papillary muscles contract as well, pulling on the chordae tendineae, closing the valves and preventing blood flow from the ventricles into the atria (i.e., regurgitation). Normally, in the RV three papillary muscles can be depicted: The anterior, the posterior, and the septal papillary muscle, respectively. The LV reveals two larger papillary muscles, the anterior and posterior papillary muscle.
Cine SSFP LA and SA images, as well as transverse images are all well suited for depicting morphology and function of the valvular apparatus. The valve leaflets can be depicted if spatial resolution is adequate. Dedicated acquisitions of specific valvular planes are used to image the valve area, which is especially useful when studying aortic valve competence. Both SSFP as well as fast gradient-echo sequences are used. Papillary muscles are well visualized on both cine brightblood as well as black-blood sequences. Chordae tendineae, on the other hand, are usually not sufficiently visualized by MRI due to the limited spatial resolution.

(Ultra -) High-Field Imaging

A decade ago, high-field 3-T whole-body MRI scanners have been introduced in clinical practice. Past studies reported 20% to 150% improvement in signal-to-noise ratio (SNR) for SSFP acquisitions at 3-T MRI when compared to 1.5 T,[13] but with the increase in field strength an increasing effect of imaging artifacts also occurred. For CMR imaging, SSFP techniques have been implemented at 3 T and optimized,[14] but especially SSFP sequences are more prone to field inhomogeneities, resulting in artifacts that may hamper image evaluation. The major source of artifact is off-resonance effects that become more pronounced at higher field strength.[15] Effective shimming of the B_0 magnetic field is paramount, but the heart is a difficult organ to shim owing to the complex field patterns in that region of the body (e.g., due to the lungs and liver).[16] Dedicated shim systems providing higher-order, cardiacphase–specific shimming have reported improved field homogeneity across the heart,[17] but currently, SSFP at high field remains not 100% reliable for use in CMR imaging. Alternative to SSFP sequences, multiple-phase fast gradient-echo sequences without SSFP may be used at high-field 3-T MRI or beyond.
Feasibility of CMR imaging at ultra-high–field 7-T MRI was first demonstrated by Snyder et al..[18] Besides the above-mentioned susceptibility artifacts, that are even more pronounced at 7 T, radio-frequency (RF) heating effects will limit the application

of SSFP at ultra-high–field even further. The specific absorption rate (SAR) level increases by the square of the field strength, and therefore, the use of SSFP has not yet been demonstrated at 7 T. Brandts et al. showed the feasibility of assessing LV volumes, function, and atrial–ventricular flow at 7-T MRI using standard multislice, multiphase cine gradient-echo and phase-contrast techniques, and they demonstrated similar quantitative results as compared to the gold standard of 1.5-T CMR.[19] Still, without the availability of dedicated hardware such as dedicated transmit/receive coils, and optimized imaging techniques, CMR at 7 T will remain an area of research.

References

1. Lenz GW, Haacke EM, White RD. Retrospective cardiac gating: A review of technical aspects and future directions. *Magn Reson Imaging.* 1989;7(5):445–455.
2. Ho SY, Nihoyannopoulos P. Anatomy, echocardiography, and normal right ventricular dimensions. *Heart.* 2006;92:I2–I13.
3. Cerqueira MD, Weismann NJ, Dilsizian V, et al. Standardized myocardial segmentation and nomenclature for tomographic imaging of the heart: A statement for healthcare professionals from the Cardiac Imaging Committee of the Council on Clinical Cardiology of the American Heart Association. *Circulation.* 2002;105:539–542.
4. Uribe S, Muthurangu V, Boubertakh R, et al. Whole-heart cine MRI using real-time respiratory self-gating. *MRM.* 2007;57:606–613.
5. Danilouchkine M, Westenberg J, Reiber J, et al. Accuracy of short-axis cardiac MRI automatically derived from scout acquisitions in free-breathing and breath-holding modes. *MAGMA.* 2005;18:7–18.
6. Miller S, Simonetti OP, Carr J, et al. MR imaging of the heart with cine true fast imaging with steady-state precession: Influence of spatial and temporal resolutions on left ventricular functional parameters. *Radiology.* 2002;223:263–269.
7. Kramer CM, Barkhausen J, Flamm SD, et al. Standardized cardiovascular magnetic resonance imaging (CMR) protocols, society for cardiovascular magnetic resonance: Board of trustees task force on standardized protocols. *J Cardiovasc Magn Reson.* 2008;10:10–35.
8. Alfakih K, Plein S, Bloomer T, et al. Comparison of right ventricular volume measurements between axial and short axis orientation using steady-state free precession magnetic resonance imaging. *J Magn Reson Imaging.* 2003;18:25–32.
9. Schneider B, Hofmaan T, Justen MH, et al. Chiari's network: Normal variant or risk factor for arterial embolic events. *J Am Coll Cardiol.* 1995;26:203–210.
10. Mansour M, Holmvang G, Sosnovik D, et al. Assessment of pulmonary vein anatomic variability by magnetic resonance imaging: Implications for catheter ablation techniques for atrial fibrillation. *J Cardiovasc Electrophysiol.* 2004;15(4):387–393.
11. Van der Voort PH, van den Bosch HCM, Post JC, et al. Determination of the spatial orientation and shape of pulmonary vein ostia by contrast-enhanced magnetic resonance angiogrpahy. *Europace.* 2006;8(1):1–6.
12. Stevenhagen J, van der Voort PH, Dekker LRC, et al. Three-dimensional CT overlay in comparison to Cartomerge for pulmonary vein antrum isolation. *J Cardiovasc Electrophysiol.* 2010;21:634–639.
13. Hinton DP, Wald LL, Pitts J, et al. Comparison of cardiac MRI on 1.5 and 3.0 Tesla clinical whole body systems. *Invest Radiol.* 2003;38:436–442.
14. Schär M, Kozerke S, Fischer S, et al. Cardiac SSFP imaging at 3 Tesla. *MRM.* 2004;51:799–806.
15. Tyler DJ, Hudsmith LE, Petersen SE, et al. Cardiac cine MR-imaging at 3 T: FLASH vs. SSFP. *J Cardiovasc Magn Reson.* 2006;8(5):709–715.
16. Atalay MK, Poncelet BP, Kantor HL, et al. Cardiac susceptibility artifacts arising from the heart–lung interface. *Magn Reson Med.* 2001;45:341–345.
17. Kubach MR, Bornstedt A, Hombach V, et al. Cardiac phase-specific shimming (CPSS) for SSFP MR cine imaging at 3 T. *Phys Med Biol.* 2009;54(20):N467–N478.
18. Snyder CJ, DelaBarre L, Metzger GJ,et al. Initial results of cardiac imaging at 7 Tesla. *Magn Reson Med.* 2009;61:517–524.
19. Brandts A, Westenberg JJ, Versluis MJ, et al. Quantitative assessment of left ventricular function in humans at 7 T. *Magn Reson Med.* 2010;64(5):1471–1477.